

Impedance behavior of nanoporous SiC

Alberto A. Sagüés^{a,*}, John T. Wolan^b, Agustin De Fex^a, Timothy J. Fawcett^b

^a Department of Civil and Environmental Engineering, University of South Florida, Tampa, FL 33620, USA

^b Department of Chemical Engineering, University of South Florida, Tampa, FL 33620, USA

Received 23 June 2004; received in revised form 16 November 2004; accepted 25 February 2005

Available online 24 August 2005

Abstract

A study was conducted of the electrochemical impedance spectroscopy (EIS) response of n-type ($\sim 10^{18} \text{ cm}^{-3}$ donor density) nanoporous 6H-SiC (PSC) with a $\sim 2000 \text{ nm}$ porous layer created by anodic HF etching and non-porous SiC (NSC) controls in NaCl and Na_2SO_4 electrolytes. At intermediate potentials, PSC had much larger interfacial capacitance than the controls, consistent with the large effective area of the porous material. At high frequencies, the PSC showed transmission line behavior in approximate agreement with predictions of a simplified model that considered the extent and size of porosity and the properties of electrolyte and interface.

© 2005 Elsevier Ltd. All rights reserved.

Keywords: Impedance behavior; Nanoporous SiC; Electrochemical impedance spectroscopy

1. Introduction

Nanoporous SiC (PSC) obtained by photo-assisted anodic etching combines desirable properties, such as wide bandgap and enhanced photoluminescence [1] and may be a useful substrate for growing improved epitaxial layers [2]. A thin (e.g. $\sim 20\text{--}100 \text{ nm}$) skin of much lower porosity may exist over the porous zone and can be stripped by reactive ion etching (RIE). Electrochemical impedance spectroscopy (EIS) tests show that in an electrolyte, the interfacial capacitance of PSC polarized moderately above the flat band potential (E_{FB}) can be much greater than the capacitance of non-porous silicon carbide (NSC) under similar conditions [3]. This observation has been interpreted as resulting from the greater effective surface area of the porous material. In contrast, EIS of metal–PSC interfaces has shown a large decrease in apparent capacitance that has been attributed variously to lower average volumetric donor dopant density because of the pores [4] or to a compensation of donor dopants by electrons in deep level surface states [5]. Additional EIS experiments are presented here to supplement the limited information available on these issues.

2. Methodology

All specimens were fabricated from a commercial n-type 6H-SiC single crystal wafer ($\sim 800 \mu\text{m}$ thick) oriented on-axis in the [000 1] direction with carrier concentrations in the range of 10^{18} cm^{-3} , resulting in room temperature resistivity of $\sim 0.05 \Omega \text{ cm}$. The PSC was created on one-half the Si-face [6] of the wafer by UV-assisted anodization in aqueous HF [7]. Some variability of properties over the treated surface was expected and may account for observed sample-to-sample response variations noted below. An outer “skin” layer of almost pore-free single crystal SiC on top of the PSC was removed over much of the specimen area by RIE with a $\text{SF}_6\text{--O}_2\text{--H}_2$ -based plasma at a removal rate of $\sim 20 \text{ nm/min}$ for 2 min. Fig. 1 shows a cross sectional scanning electron microscope (SEM) image of the resulting wafer, revealing a $\sim 2000 \text{ nm}$ deep pore zone with “chevron”-type pore morphology [8]. Typically, pore trace width was $\sim 30 \text{ nm}$ and pores were $\sim 100\text{--}200 \text{ nm}$ apart, total volumetric porosity was visually estimated to be in the order of 5–10%. This morphology is among those reported for PSC by other investigators [5,8]. The other half of the wafer was not subject to anodization to serve as a control, parts of it were used as-received and others subject to RIE in the same manner as the PSC.

* Corresponding author.

E-mail address: sagues@eng.usf.edu (A.A. Sagüés).

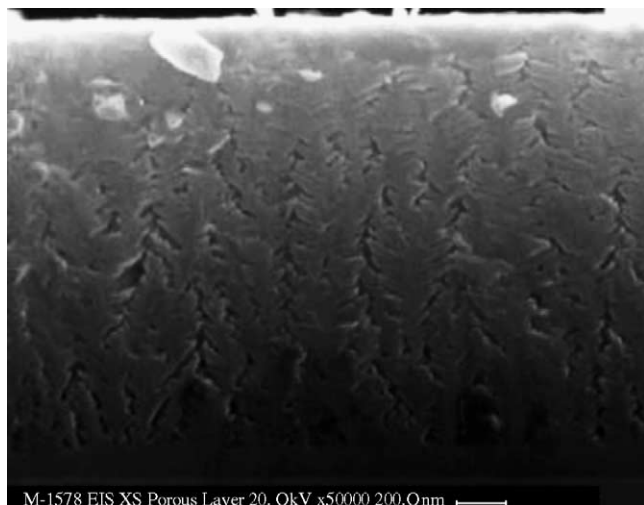


Fig. 1. Cross section SEM image of the porous region showing remnants of “skin” zone at top and chevron-shaped porosity with termination front ~ 2000 nm below the surface.

Portions of each side of the wafer were cut into roughly square duplicate specimens ~ 15 mm on the side. Ni–Cr (80–20) alloy strips ~ 2 mm wide and ~ 0.2 μm thick were deposited via electron beam evaporation near opposite edges of the sample on the Si-face. Each specimen was then annealed in a rapid thermal processing chamber under an Ar atmosphere for 2 min at 950°C to achieve ohmic contact between the strips and the substrate. Except for one of the PSC specimens, the first RIE treatment was applied before depositing and annealing the contacts. Some samples were subjected to an additional RIE treatment (but no further contact annealing) after an initial characterization by EIS had taken place.

EIS and dc polarization experiments were conducted on the interface between the finished PSC or control and various aqueous electrolytes. The electrolytes were naturally aerated, neutral pH solutions of NaCl (0.06, 0.17 M) or Na_2SO_4 (0.17 M) in distilled water. All electrochemical measurements were performed under dark conditions at $\sim 22 \pm 2^\circ\text{C}$.

Fig. 2 shows the test cell arrangement. Electrolyte (~ 0.5 cm^3 , ~ 0.3 cm^2 contact area) was placed in a plastic tube attached to the specimen face with epoxy adhesive. Connections were made to the ohmic contact strips, one of which served as the current insertion and the other as a potential sensing terminal of the working electrode. This arrangement minimized effects of any polarization that may have taken place at the current insertion connection of the working electrode. A ~ 1 mm wide Ti wire activated with an outer mixed-metal-oxide surface layer [9] was inserted in the electrolyte to a depth of ~ 5 mm to serve as counter electrode. The reference electrode was a miniature Ag/AgCl electrode which permitted EIS measurements with little spurious capacitance effects up to 3×10^4 Hz. The usable range was extended to ~ 200 kHz in selected measurements by using instead another activated Ti wire electrode as a low

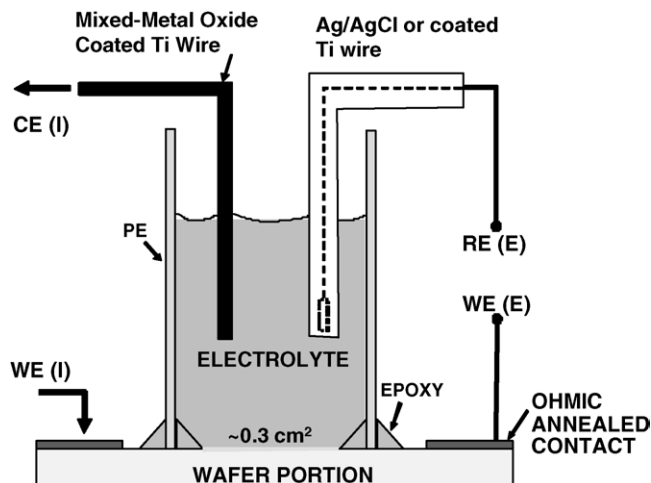


Fig. 2. Schematic of test cell arrangement. For reporting purposes, all potentials have been converted to the SCE scale.

impedance reference electrode, previously calibrated against the Ag/AgCl electrode. In all cases, potentials have been converted to the saturated calomel electrode (SCE) scale for reporting purposes. Before attaching the plastic tube to the specimen, its surface was cleaned with acetone, rinsed with isopropanol and allowed to dry. The epoxy was cured for 1 day before placing the solution in the cell. The electrochemical measurements were acquired typically starting about 1 h after placing the solution in contact with the specimen.

Frequency dispersion EIS data were usually collected using an excitation of 10 mV rms, from 10^{-2} Hz up to the useable high frequency limit of the reference electrode chosen. Mott–Schottky (M–S) measurements were performed usually at $-1\text{ V} < E < 1\text{ V}$ and 1 kHz (and in some cases also at 100 Hz and 10 kHz) with an amplitude of 10 mV and scan rate of 1 mV/s. Cyclic potentiodynamic scans were conducted at a scan rate of 2 mV/s. Experiments at $E < -1\text{ V}$ were deemed to be little productive due to the onset of water decomposition and thus not conducted. All tests were made with a Solartron 1260/1287 potentiostat/electrochemical interface.

3. Results

3.1. Quasi-static polarization behavior

Figs. 3 and 4 show the potentiodynamic response of NSC and PSC, respectively, in 0.17 M NaCl. Instrumentation resolution at the settings used caused current uncertainty in the order of $\sim 10^{-10}$ to 10^{-9} A/cm^2 . Comparable behavior was observed in the other electrolytes and concentrations examined. At potentials higher than approximately -0.4 V , net oxidation or reduction rates were very small (typically $|\text{current density}| < \sim 10^{-8}$ A/cm^2). At these potentials, current fluctuation above instrumentation noise was noted in some cases (e.g. Fig. 4) but the cause has not been identified. At more negative potentials, a cathodic reaction became dominant with an

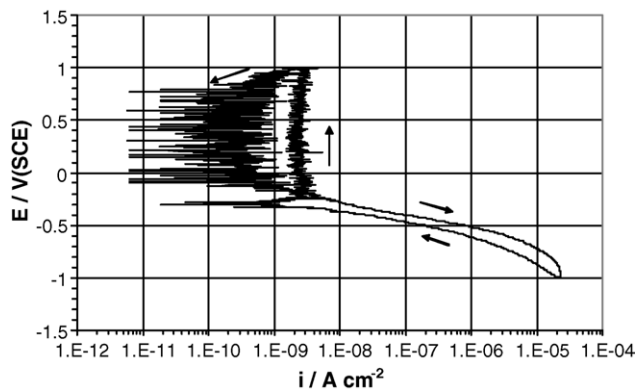


Fig. 3. Potentiodynamic response of NSC in 0.06 M NaCl.

apparent Tafel slope of $\sim 100\text{--}200$ mV/decade and seemingly approaching a diffusion-limited regime with current density $i_L \sim 10^{-5}$ A/cm². Selected experiments in which the entire test cell was placed in a N₂-blanketed container yielded i_L values that were one to two orders of magnitude lower.

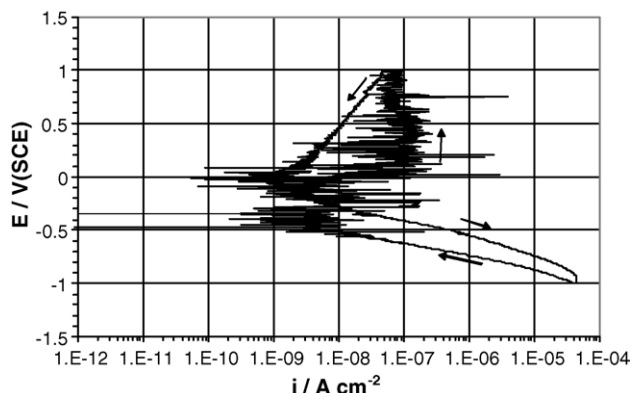


Fig. 4. Potentiodynamic response of PSC in 0.06 M NaCl.

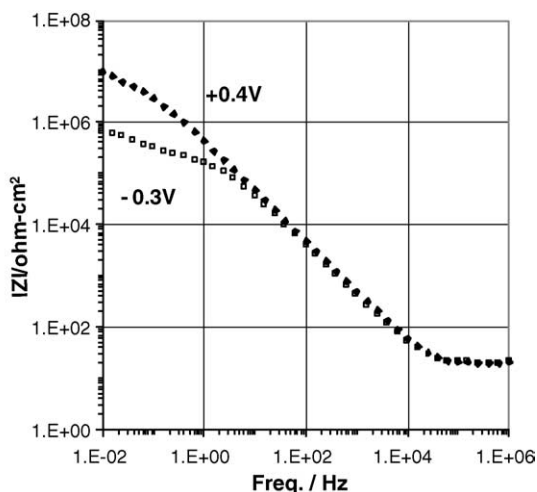
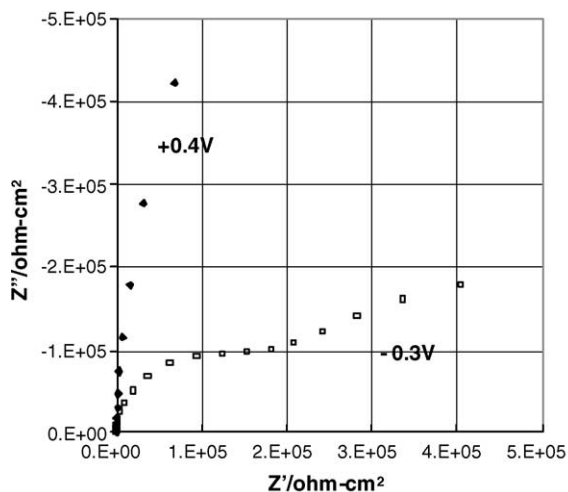


Fig. 5. EIS behavior of NSC (surface area 0.23 cm²) in 0.17 M NaCl at two different polarization regimes.

3.2. EIS – Mott–Schottky plots and intermediate frequency response

Typical EIS spectra obtained for NSC and PSC in 0.17 M NaCl at different potentials are shown in Figs. 5 and 6, respectively. The solution resistance value observed at high frequencies was consistent with the cell dimensions and the value of the electrolyte conductivity. Besides the solution resistance, the EIS response at frequencies $> \sim 1$ Hz was dominated by a near-ideal capacitive component and a small, nearly ohmic polarization admittance that increased at potentials where the cathodic reaction noted above was also important. At low frequencies and low potentials, the impedance behavior was dominated by electrode reactions. The EIS behavior for a given surface condition was comparable for all concentrations and both types of electrolyte used.

The nearly capacitive-solution resistance response at high frequencies can be further simplified as being modeled by a simple resistor–capacitor series equivalent circuit (the low frequency response of the system is ignored). Such approximation is made by software built in the test instrumentation when it is in the M–S measuring mode, which then reports the resulting capacitance value C . Fig. 7 shows the 1 kHz M–S results for the three surface conditions in 0.17 M NaCl. The observed trends were similar in the other electrolytes and at the other frequencies tested. The surface-normalized value of C^2 increased with potential, in a manner consistent with the establishment of a space charge zone in an n-type semiconductor [1,10]. In all test conditions, the C^2 versus E dependence became nearly linear at the higher potentials (selected tests performed up to $E = 2$ V showed that the slope did not change in that range). The value of the effective donor density N_d can be evaluated from the high potential slope S of the M–S plot by $N_d = 2/\epsilon\epsilon_0q_eS$ [10], where ϵ_0 is the permittivity of free space (8.85×10^{-14} F/cm), q_e the elementary charge (1.6×10^{-19} C) and ϵ is the relative dielectric constant of SiC (9.7 [11]). While there was variability in the results of

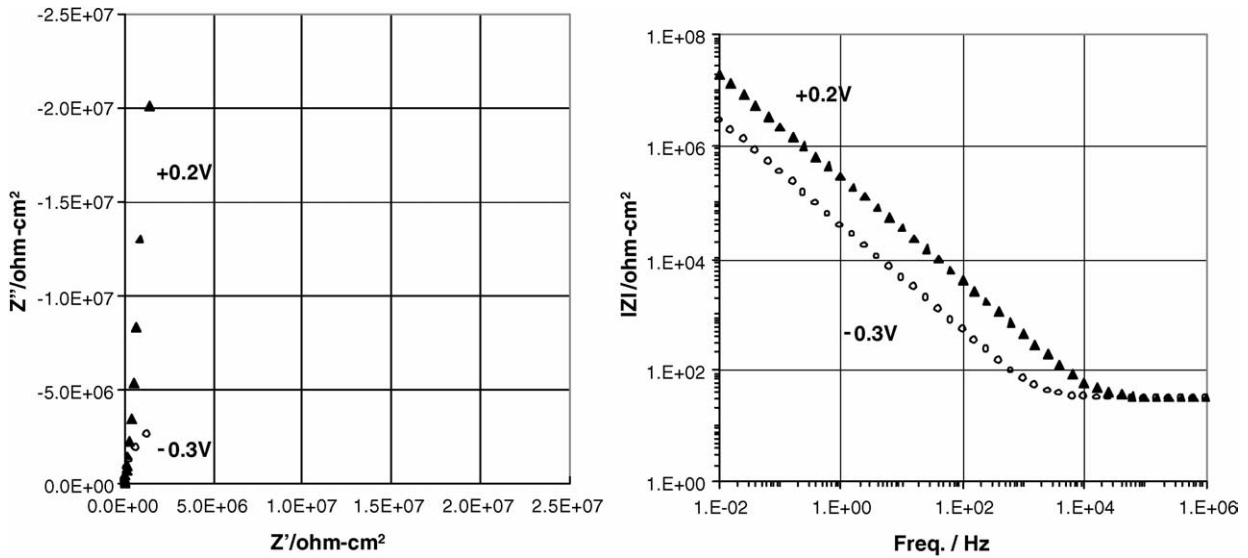


Fig. 6. EIS behavior of PSC (0.36 cm²) in 0.17 M NaCl at two different polarization regimes.

duplicate samples, N_d was comparable for all three surface conditions (Fig. 8) and in the order of the 10^{18} cm^{-3} reported by the wafer manufacturer. Extrapolation of the linear region to intersection with the potential axis yielded nominal flat band potentials (E_{FB}) in the order of -1.1 to -1.5 V , consistent with the range of values reported elsewhere for n-doped SiC [1].

At the more negative potentials, there was significant deviation from the M–S behavior expected from a simple depletion zone for all three material conditions. Both the untreated NSC and the NSC subject to RIE showed abrupt increases in capacitance at potentials that approached the nominal E_{FB} . A similar but more pronounced deviation, and at higher potentials ($E \sim 0$ – 0.3 V), was observed for the PSC specimens.

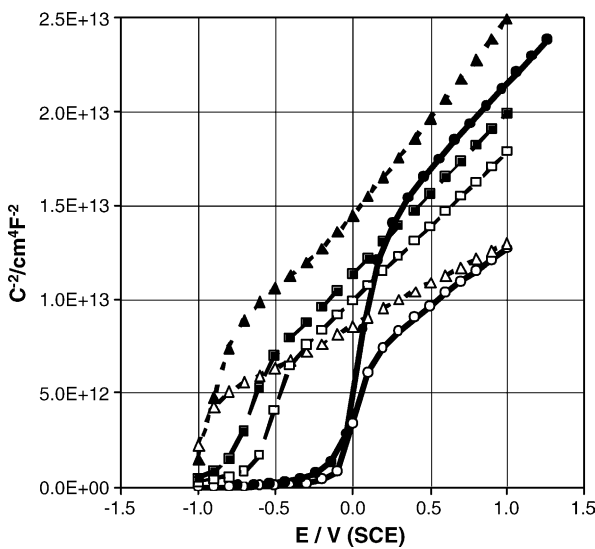


Fig. 7. Inverse square 1 kHz capacitance–potential (Mott–Schottky) behavior in 0.17 M NaCl for tests in duplicate. (Circles) PSC; (triangles) NSC after RIE; (squares) NSC as-received.

The EIS spectra were analyzed to improve upon the idealized capacitance estimates returned by the simple R – C M–S analyses. In the following impedance/admittance terms are understood to be area-normalized whenever appropriate. It was found that in the frequency interval of 30 kHz–100 Hz, the EIS response could be accurately represented with an equivalent circuit consisting of a solution resistance in series with a parallel combination of a nominal polarization admittance and a constant-phase angle-element (CPE) [12] with admittance $Y_{CPE} = Y_0(j\omega)^n$ where Y_0 and n are the CPE parameters. Typical results (0.17 M NaCl) are shown in Figs. 9 and 10; results for the other electrolytes were comparable. Fig. 9 shows that the CPE at high potentials was very close to ideal behavior ($n \sim 0.98$ – 0.98) for NSC, but slightly less so ($n \sim 0.95$) for PSC. There was greater but still only modest deviation from ideality ($n > \sim 0.8$) at the lower

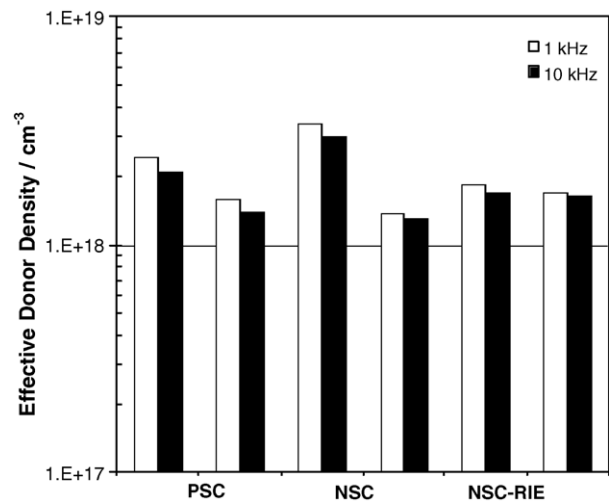


Fig. 8. Effective donor density estimated from high potential slope of M–S plots of tests in 0.17 M NaCl.

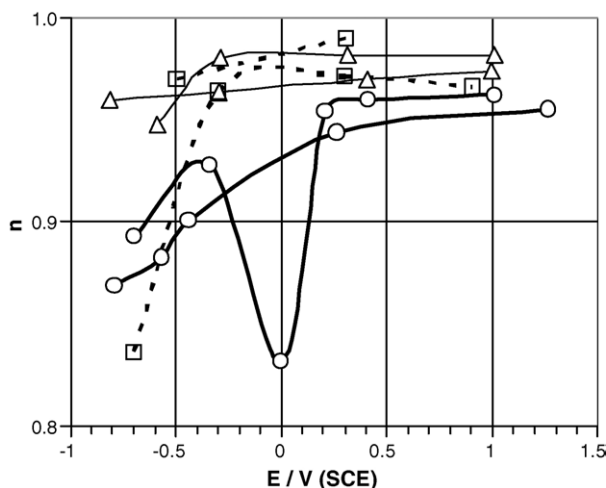


Fig. 9. CPE exponent n as function of potential in 0.17 M NaCl. Duplicate specimens. (Circles) PSC; (triangles) NSC after RIE; (squares) NSC as-received.

potentials. Therefore, in all cases, Y_0^* (the numeric value of Y_0 in F/cm^2) could be viewed as an approximate interfacial capacitance. In all cases at high potentials, Y_0^* was in the order $10^{-7} \text{ F}/\text{cm}^2$, consistent with the space charge layer behavior examined earlier. Y_0^* values more than one order of magnitude greater were reached for PSC as potentials became more negative than $\sim 0 \text{ V}$. The NSC-RIE specimens tended to reach comparably high Y_0^* values but at more negative potentials. These observations match the capacitance trends derived from the M–S analysis, including the weak dependence on test frequency at high potentials which is consistent with the near-unity values of n observed by EIS.

It is noted that the Y_0^* values obtained actually reflect the series combination of the capacitance on the semiconductor side with the double layer capacitance C_{DL} . However, C_{DL} is typically in the order of $20 \mu\text{F}/\text{cm}^2$ for a flat surface

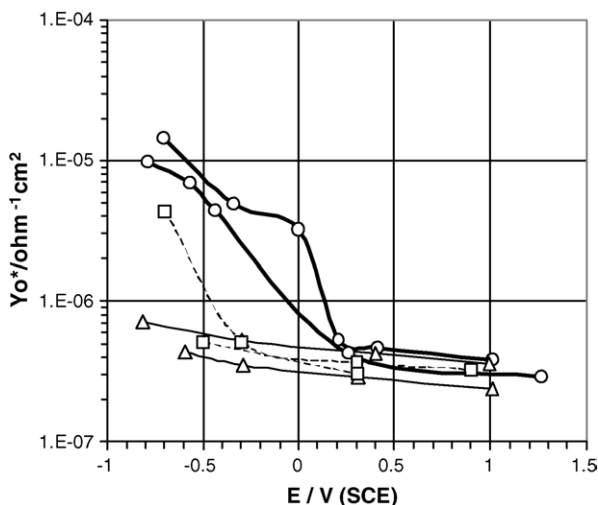


Fig. 10. Area-normalized CPE parameter Y_0^* as function of potential in 0.17 M NaCl. Duplicate specimens. (Circles) PSC; (triangles) NSC after RIE; (squares) NSC as-received.

[13], which is still about one order of magnitude greater than the largest Y_0^* values observed for NSC-RIE in the potential range examined, so its contribution in that case is likely negligible. A similar argument applies to PSC where the Y_0^* values were higher, but C_{DL} should also be greater because of the increased surface area.¹

3.3. EIS—high frequency response

Fig. 11 shows the high frequency EIS behavior under approximately -0.5 V polarization in NaCl solutions obtained using the Ti wire reference electrode. The Na_2SO_4 experiments yielded comparable results. The NSC specimens either as-received or after RIE showed nearly ideal capacitive behavior. In contrast, despite some specimen-to-specimen variability, the PSC showed an $\sim 45^\circ$ phase angle, after compensating for the solution resistance, at the highest test frequencies before a transition to behavior similar to the NSC at lower frequencies (note diagrams are staggered for clarity, by adding multiples $5 \Omega \text{ cm}^2$ to the real axis of each after compensating for solution resistance). For both PSC specimens, the low angle region was larger in the Nyquist diagram when the electrolyte was more dilute. At potentials $> \sim 0.3 \text{ V}$, the high frequency impedance diagrams of PSC did not show a pronounced low angle region and resembled more those of an ideal capacitance.

4. Discussion

A clear differentiation between electrochemical behavior of porous and non-porous surfaces was in the increased apparent capacitance of the latter at potentials below $\sim 0.3 \text{ V}$; van de Lagemaat [3] proposed that the effect is important only at low potentials when the width w of the depletion zone is small enough that it can follow the contour of the pore surface. At higher potentials, the depleted zones of adjacent pores would merge into a front (placed below the porosity front in Fig. 1) with surface area equal to the macroscopic value. The capacitance–potential behavior at those potentials would then be similar to that of a non-porous SiC specimen.

The measurements and parameters of the present system generally agree with the above interpretation. The increase in area on PSC is large since even if the pores were simply cylindrical in shape, the dimensions indicated earlier ($\sim 150 \text{ nm}$ apart, $\sim 30 \text{ nm}$ wide and $\sim 2000 \text{ nm}$ deep) would correspond to an increase of a factor of ~ 10 over the area of an ideally flat surface. The tortuous nature of the actual porosity (considered later on) suggests that the actual difference is even larger. The width w of the depletion zone can be estimated by $w = (2\varepsilon\varepsilon_0(E - E_{\text{FB}} - kTq_e^{-1})/q_eN_{\text{D}})^{1/2}$ (where $k = 1.38 \times 10^{-23} \text{ J}/\text{K}$ is Boltzmann's constant and T is the

¹ The concentrated electrolyte used in the experiments is expected to result in a compact double layer able to follow the microscopic contour and retain charge storage properties accordingly.

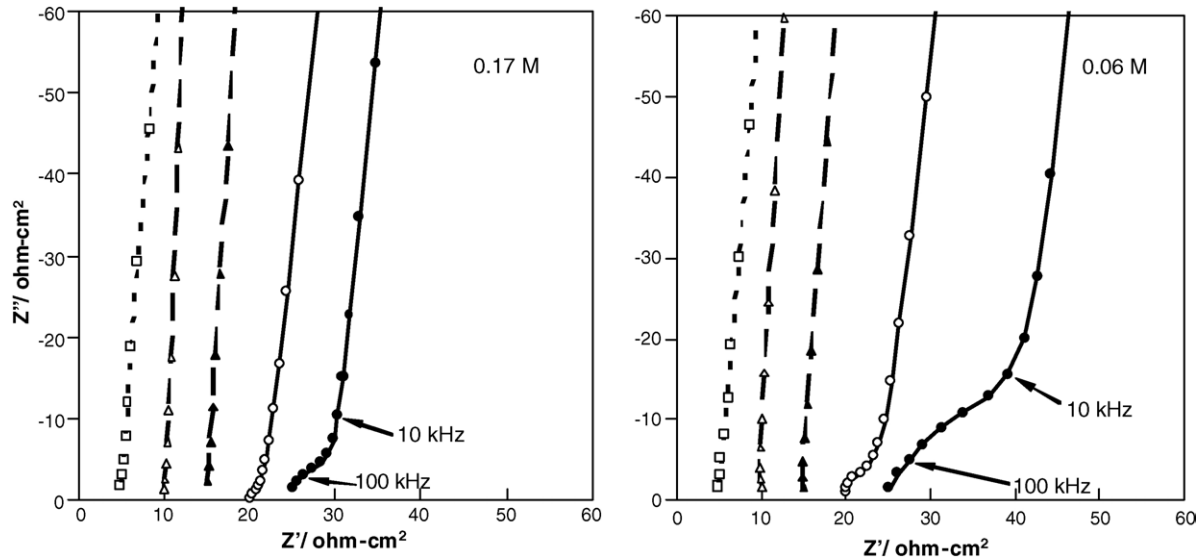


Fig. 11. High frequency impedance response of PSC and NSC in NaCl solutions. (Circles) PSC (duplicate specimens); (triangles) NSC after RIE (duplicate); (squares) NSC as-received. Zero in real axis is arbitrary after subtracting solution resistance; diagrams are staggered $5 \Omega \text{ cm}^2$ apart for clarity. Highest test frequency is 250 kHz. Tests performed at 5 points/decade, key frequencies indicated on rightmost plot.

absolute temperature) [10], which for the present case yields $w \sim 16 \text{ nm}$ at $E = -1 \text{ V}$, but $w \sim 30 \text{ nm}$ at $+0.5 \text{ V}$, approaching the half-distance between pores.

Some caution is necessary in adopting the above scenario. For example, NSC subjected to RIE had a capacitance transition at a potential nearly halfway between that of untreated NSC and PSC, suggesting that the capacitance increase in PSC could be due at least in part to the introduction of a high population of surface states [1,10,14] during processing, rather than solely to an increase in geometric area. Conversely, if deep level traps were responsible for much of the capacitance increase, the broad potential range covered by the increase would imply that the trap energies should span an unusually wide range [14]. The role of surface states is discussed further below.

Another issue implicit in the above interpretation of the results is the assumption that electrolyte is actually penetrating the pores. The electrolytes used did wet the PSC surface, as indicated by macroscopic observation of acute contact angles in test droplets. If wetting extends also at the microscopic level, capillary pressures (in the order of $2\gamma/r$, where γ is the surface tension of water and r is the pore radius) should greatly exceed atmospheric pressure, and therefore, allow for deep penetration of the pores upon electrolyte placement in the cell even with initially air-filled pores. Electrolyte contact appears then to be reasonably expected to have occurred but it is uncertain to which extent, this is considered briefly next.

There was also clear differentiation between PSC and NSC in their high frequency response. Interfacial porosity is known to cause deviation from ideal capacitive behavior as a result of establishment of a truncated transmission line configuration coupling the longitudinal electrolyte resistance along the pores with the capacitive admittance on the pore walls [15].

In the simplest case and without other electrode reactions, the impedance Z_p of a uniform cross section pore is given by:

$$Z_p = \frac{(RY^{-1})^{1/2}}{\tanh(L(RY)^{1/2})} \quad (1)$$

where R and Y are, respectively, the unit length resistance and unit length pore wall admittance of the pore and L is the pore length. The resulting impedance has a 45° phase angle at high frequencies, and below a transition frequency f_T , the phase angle approaches 90° as in an ideal capacitor but with a limiting real impedance component R_{LIM} . The high frequency EIS response in Fig. 11 resembles that behavior and it was examined by the model described next.

For simplicity, the pores are considered to be uniformly filiform and tortuous with round cross section and effective length $L = L_0\tau^{1/2}$ where L_0 is the depth of the porous zone and τ is the tortuosity [17]. The total volume fraction porosity is P . The pores are separated from each other by a distance h on a uniform square grid, so the pore diameter is $2h(P/\tau\pi)^{1/2}$. The pores are assumed to be filled with electrolyte of resistivity ρ and the interfacial capacitance per unit area along the pore walls is C_0 (same as the unit capacitance of a non-porous surface). The resulting unit length resistance and capacitive admittance are, respectively,

$$R = \frac{\rho\tau^{1/2}}{Ph^2} \quad (2)$$

$$Y = 2j\omega C_0 h \left(\frac{P\pi}{\tau^{1/2}} \right)^{1/2} \quad (3)$$

The total admittance Y_T per unit area of semiconductor/electrolyte interface is the parallel combination of the

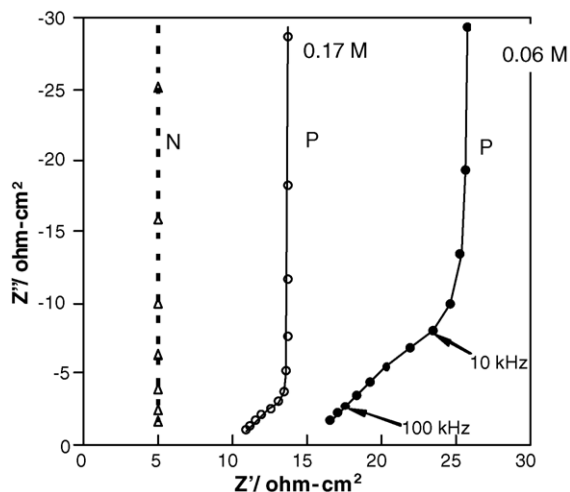


Fig. 12. Simplified model output for PSC (P) in NaCl solutions and NSC (N) using input parameters as indicated in the text. Diagrams staggered and denoted as in Fig. 11.

admittance of all pores and the admittance of the portion of the interface not covered by pores (fraction $1-P$ [17]), assumed to be capacitive as well in the same manner as the pore walls. Thus, the corresponding impedance $Z_T = Y_T^{-1}$ is

$$Z_T = (Z_p^{-1}h^2 + j\omega C_o(1-P))^{-1} \quad (4)$$

The form of the above equations implies that the real component of the vertical branch of the impedance diagram is

$$R_{LIM} = \frac{\rho L_o \tau}{3P} \quad (5)$$

If only a fraction f_p of the pores is effectively filled with electrolyte, both Z_p and R_{LIM} become greater by a factor f_p^{-1} .

Impedance diagrams were calculated per Eq. (4) for cases assuming $\rho = 60$ and $170 \Omega \text{ cm}$ (representative of the room temperature resistivity of 0.17 and 0.06 M NaCl solutions, respectively), $C_o = 0.4 \mu\text{F}/\text{cm}^2$ (typical of the space charge region capacity observed at high potentials, Fig. 10) and $L_o = 2000 \text{ nm}$, $h = 120 \text{ nm}$ and $P = 0.05$ (representative of the appearance of the pore zone in Fig. 1). These assumptions yield pore diameters ranging from ~ 30 to $\sim 15 \text{ nm}$ for $\tau^{1/2} = 1-4$, respectively, also representative of Fig. 1. Initial calculations indicated that for $\tau^{1/2} = 1$ and $f_p = 1$, the value of R_{LIM} was much smaller than suggested by the results in Fig. 11. However, assuming still plausible values of $\tau^{1/2} = 4$ and $f_p = 1/3$ resulted in the example modeled output shown in Fig. 12, which approximates the observed behavior illustrating as well the increase in R_{LIM} as electrolyte resistivity increases. Even with the assumed value of f_p , the total apparent capacitance is still about one of order of magnitude greater than that of the ideally non-porous case.

The model involves sweeping simplifications and its output serves only as a semiquantitative indication that EIS measurements have potential for characterizing the extent

and morphology of porosity in PSC. Factors other than those considered above could also account for the observed behavior. For example, the effective value of C_o may be different than assumed because of the difference between electric field distribution around narrow pores and that of a flat surface; effective conductivity of the electrolyte may vary as well in a narrow channel compared with the bulk value used. The observations and the model indicate that high test frequencies are needed for characterizing this type of porosity as the transition frequency f_T , which is in the order of $1/RCL^2$ [15,16] falls in the order of tens to hundreds of kHz. Measurements with a cell optimized for MHz-range tests are needed, as well as models that include the effect of complex pore geometry [18], ionic transport in narrow channels and multidimensional development of the space charge zone. Other complicating factors are noted elsewhere [19,20].

The quasi-static polarization behavior (Figs. 3 and 4) of both the NSC and PSC interfaces was consistent with the expectation of nearly insulating behavior at high potentials, providing little support for net electrode reactions. At low enough potentials, there was enough electron transfer taking place to support an appreciable cathodic reaction rate. The cathodic reaction was most likely oxygen reduction, based on the apparent Tafel slope and on the observed value of i_L and its decrease upon deaeration [21]. There was relatively little differentiation between NSC and PSC in these experiments. This is not surprising at high potentials, if merging of depletion zones there renders both materials similar, but at intermediate potentials in the apparent Tafel regime (before the establishment of a macroscopic transport pattern in the liquid at very negative potentials [21]), one may have expected greater cathodic current in the porous material at least. Possible limiting causes needing future consideration include ohmic potential drop in the pores, insufficient diffusional oxygen delivery into the pore and development of an in-pore environment not propitious for the cathodic reaction.

Finally, the present and previous [3] observations with NSC in electrolytes contrast with recent reports [4,5] of metal/n-SC Schottky junctions having a much reduced space charge capacitance on PSC compared to NSC. This is not completely unexpected since in a metal-SC junction there is no contact penetration into the pores (even in the case of a non-pressurized mercury probe, as no wetting exists). Soloviev et al. ascribed the capacitance lowering, by as much as three orders of magnitude, to an effective average reduction of N_D in PSC due to the empty pore space. Ivanov et al. [5] observed a similar effect but argued that volumetric reduction in effective N_D alone could not explain the large effect observed (although these authors appeared not to have considered the multiplying effect of a simultaneous reduction in effective dielectric constant). They postulated instead that populated deep level electron surface states, on average volumetrically distributed in the porous layer, contributed to greatly lowering the average value of N_D there. This explanation however requires that the levels of those surface states be such that no significant excitation occurred in the

potential range they examined (which was several V) and that the effective density of surface states be coincidentally quite close to that of the initial N_D . Parallel characterization of PSC with electrolytic and metallic contacts should be conducted to elucidate the validity of these hypotheses.

5. Conclusions

Nanoporous silicon carbide showed greatly increased interfacial capacitance compared with non-porous silicon carbide. The effect took place at moderately negative polarization potentials where the space charge layer was expected to be thin compared to the interpore spacing, in agreement with previously proposed mechanisms. However, surface states may play a partial role in establishing the relative response of PSC and NSC. Samples of NSC subject to reactive ion etching showed also a transition to higher capacitance but at more negative potentials.

Additional differentiation between PSC and NSC was manifested by transmission line behavior of the porous material at high frequency. There was semiquantitative agreement between the observed behavior and the predictions of a simplified model that considered the extent and size of porosity and the properties of electrolyte and interface.

References

- [1] J. van de Lagemaat, D. Vanmaekelbergh, J.J. Kelly, *J. Appl. Phys.* 83 (1998) 6089.
- [2] M. Mynbaeva, S.E. Sadow, G. Melnychuk, I. Nikitina, M. Scheglov, A. Sitnikova, N. Kuznetsov, K. Mynbaev, V. Dmitriev, *Appl. Phys. Lett.* 78 (2001) 117.
- [3] J. van de Lagemaat, M. Plakman, D. Vanmaekelbergh, J.J. Kelly, *Appl. Phys. Lett.* 69 (1996) 2246.
- [4] S. Soloviev, T. Das, T.S. Sudarshan, *Electrochem. Solid-State Lett.* 6 (2003) 22.
- [5] P.A. Ivanov, M.G. Mynbaeva, S.E. Sadow, *Semicond. Sci. Technol.* 19 (2004) 319.
- [6] *Encyclopaedia of Materials, Science and Technology*, Elsevier, 2001, p. 8508.
- [7] J.E. Spanier, A.C. West, I.P. Herman, *J. Electrochem. Soc.* 148 (2001) C663.
- [8] A. Sagar, C.D. Lee, R.M. Feenstra, C.K. Inoki, T.S. Kuan, *J. Appl. Phys.* 92 (2002) 4070.
- [9] P. Castro, A.A. Sagüés, E.I. Moreno, L. Maldonado, J. Genesca, *Corrosion* 52 (1996) 609.
- [10] P. Schmuki, H. Boehni, J.A. Bardwell, *J. Electrochem. Soc.* 142 (1995) 1705.
- [11] Y. Goldberg, M. Levinshtein, S. Rumyantsev, in: Levinshtein, Rumyantsev, Shur (Eds.), *Properties of Advanced Semiconductor Materials*, J. Wiley, New York, 2001.
- [12] A.A. Sagüés, S.C. Kranc, E. Moreno, *Corros. Sci.* 37 (1995) 1097.
- [13] J. Bockris, A. Reddy, *Modern Electrochemistry*, Plenum/Rosetta, New York, 1977.
- [14] N. Sato, *Electrochemistry of Metal and Semiconductor Electrodes*, Elsevier, Amsterdam, 1998.
- [15] R. DeLevie, *Electrochim. Acta* 9 (1964) 1231.
- [16] H. Keiser, K. Beccu, M. Gutjahr, *Electrochim. Acta* 21 (1976) 539.
- [17] J. Bear, *Dynamics of Fluids in Porous Media*, Dover Publications Inc., NY, 1988.
- [18] I.D. Raistrick, *Electrochim. Acta* 35 (1990) 1579.
- [19] H. Song, J. Sung, Y. Jung, K. Lee, L. Dao, M. Kim, H. Kim, *J. Electrochem. Soc.* 151 (2004) E102.
- [20] J. Bisquert, G. Garcia-Belmonte, F. Fabregat-Santiago, N.S. Ferriols, P. Bogdanoff, E.C. Pereira, *J. Phys. Chem. B* 104 (2000) 2287.
- [21] H. Kaesche, *Metallic Corrosion*, NACE International, Houston, 1985.